

Longitudinal double-spin asymmetries of inclusive jet and dijet production at STAR

Maria Zurek^{1*} for the STAR Collaboration

¹ Argonne National Laboratory, Lemont, USA

* zurek@anl.gov

July 30, 2021



*Proceedings for the XXVIII International Workshop
on Deep-Inelastic Scattering and Related Subjects,
Stony Brook University, New York, USA, 12-16 April 2021
doi:10.21468/SciPostPhysProc.?*

Abstract

At the STAR experiment, the gluon helicity distribution $\Delta g(x, Q^2)$ can be accessed through the double-spin asymmetries A_{LL} of inclusive jet and dijet production in collisions of longitudinally polarized protons. These proceedings report on recently published results of A_{LL} for inclusive jets and dijets at $\sqrt{s} = 200$ GeV and $\sqrt{s} = 510$ GeV in mid-pseudorapidity ($|\eta| < 1$) and preliminary results for dijets in intermediate pseudorapidity ($-0.8 < \eta < 1.8$). The mid-pseudorapidity jet and dijet measurements are sensitive to $\Delta g(x, Q^2)$ for gluon momentum fractions x from $\simeq 0.5$ down to $\simeq 0.015$; the sensitivity region for dijets in intermediate pseudorapidity at 510 GeV extends to even lower x . The measurements are in good agreement with previous STAR results and recent theoretical evaluations of prior world data.

1 Introduction

How is the spin of the proton distributed among its quark, anti-quark, and gluon constituents? Decades of polarized Deep Inelastic Scattering experiments show that only about 25-30% of the proton's spin comes from the spins of quarks and anti-quarks [1–5]. The rest must originate from the the spins of the gluons and the orbital angular momenta of the quarks and gluons. The Solenoidal Tracker at Relativistic Heavy Ion Collider (STAR) experiment is addressing this fundamental question about the origin of the proton spin using collisions of high-energy polarized protons. Since gluon-gluon and gluon-quark scatterings dominate jet production at $\sqrt{s} = 200$ GeV and $\sqrt{s} = 510$ GeV at STAR, measurements of the double-spin asymmetries of inclusive jet and dijet production in longitudinally polarized proton collisions provide access to the gluon spin contribution to the proton spin.

STAR results on inclusive jet production at mid-pseudorapidity using 200 GeV p+p data collected in 2009 [6], when included in perturbative QCD (pQCD) analysis of global data, provide evidence for positive gluon polarization for the momentum fraction $x > 0.05$ at a scale $Q^2 = 10$ GeV² [1, 2]. The measurements of dijet A_{LL} based on the same data [7, 8] provide more information about the initial state kinematics and further constrain the x -dependence of the gluon polarization as shown in [3]. Perturbative QCD analyses at the next-to-leading order [1, 2] using the available world data show that spins of gluons with momentum fractions $x > 0.05$ contribute approximately 40% of the total proton spin at $Q^2 = 10$ GeV², with

a relative uncertainty of about 30%. The corresponding unpolarized differential jet and dijet production cross sections at STAR, including recent preliminary results for inclusive jets at $\sqrt{s} = 200$ GeV and 510 GeV [9, 10], are well described by next-to-leading order pQCD calculations. Further reduction on the uncertainty of $\Delta g(x, Q^2)$ at $x > 0.05$ calls for measurements with improved statistics at $\sqrt{s} = 200$ GeV, while improvements in the lower x region can be achieved with measurements at a higher center-of-mass energy $\sqrt{s} = 510$ GeV and more forward pseudorapidity up to $\eta \simeq 1.8$ at STAR.

2 Experiment and Data Analysis

In the inclusive jet and dijet A_{LL} measurements at STAR, the Time Projection Chamber [11] with a 0.5 T solenoidal magnetic field is used to measure charged particle tracks in $|\eta| < 1.3$ and full range of the azimuthal angle. Barrel (BEMC) [12] and Endcap Electromagnetic Calorimeters (EEMC) [13] measure the electromagnetic energy deposition in $|\eta| < 1$ and $1.09 < \eta < 2$, respectively, in full range of the azimuthal angle. The calorimeters are also used for jet triggers that require minimal transverse energy deposition in fixed $\Delta\eta \times \Delta\phi = 1 \times 1$ regions. Moreover, information from the Vertex Position Detectors [14] and the Zero Degree Calorimeters [15], covering $4.2 < |\eta| < 5.2$ and $|\eta| > 6.6$, respectively, is used to calculate the relative luminosities for different helicity configurations of the colliding beams.

Previously published results on inclusive jet and dijet production at $\sqrt{s} = 200$ GeV [6–8] are based on 2009 data corresponding to an integrated luminosity of $\mathcal{L} = 20 \text{ pb}^{-1}$. The recent results of the inclusive jet and dijet A_{LL} measurements at $\sqrt{s} = 200$ GeV and mid-pseudorapidity [16] presented in these proceedings are based on the longitudinally polarized data collected in 2015 with an approximately twice larger figure of merit, $\mathcal{L}P^4$, than 2009 data. It corresponds to an integrated luminosity of $\mathcal{L} \simeq 52 \text{ pb}^{-1}$ and average beam polarizations of $P_B \simeq 52\%$ and $P_Y \simeq 57\%$ for the RHIC “blue” (B) and “yellow” (Y) beams, respectively. The presented results at $\sqrt{s} = 510$ GeV [17] are based on the data collected in 2012 with an integrated luminosity $\mathcal{L} \simeq 82 \text{ pb}^{-1}$ and beam polarizations of about $P_B \simeq 54\%$ and $P_Y \simeq 55\%$.

The double spin asymmetries are evaluated according to the following formula:

$$A_{LL} = \frac{\sum_{\text{runs}} P_B P_Y (N^{++} - r N^{+-})}{\sum_{\text{runs}} P_B^2 P_Y^2 (N^{++} + r N^{+-})}, \quad (1)$$

where P_B and P_Y are the measured beam polarizations, N^{++} and N^{+-} are the yields of inclusive jets or dijets from colliding beam bunches with equal or opposite helicities, respectively, and r is the relative luminosity for collisions with these helicity configurations.

The details about the event selection, jet reconstruction, and systematic uncertainty estimation can be found in [16, 17]. One of the main improvements of the presented results with respect to previous STAR measurements [6, 7] is the jet-by-jet underlying-event correction. Jet p_T and dijet invariant mass, M_{inv} , are corrected for underlying-event contributions using the off-axis method from [18].

3 Results

The inclusive jet A_{LL} for $\sqrt{s} = 200$ GeV and $\sqrt{s} = 510$ GeV are presented in Fig. 1. Figure 1a shows the recent results at $\sqrt{s} = 200$ GeV and $|\eta| < 1$ based on 2015 data [16] together with the results using 2009 data [6]. The first results at $\sqrt{s} = 510$ GeV and $|\eta| < 0.9$ using 2012 data [17] are shown in Fig. 1b.

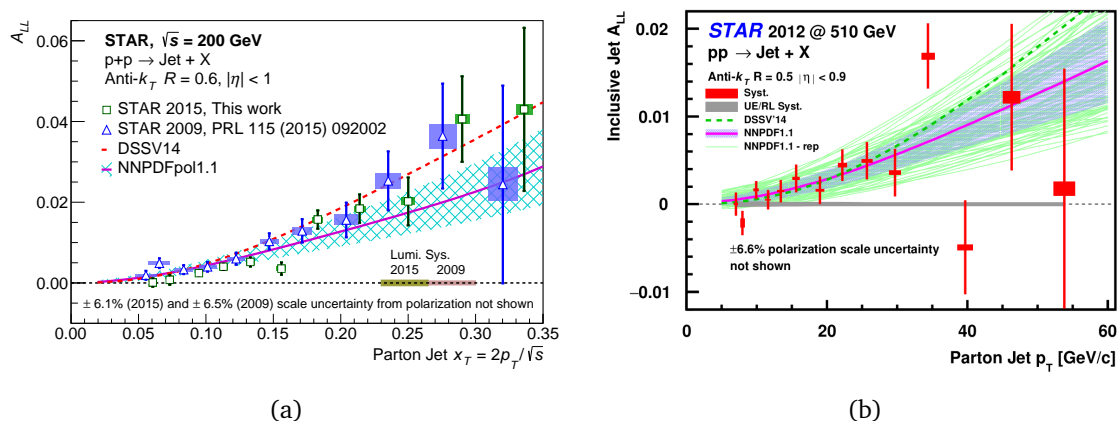


Figure 1: (a) A_{LL} for inclusive jets with $|\eta| < 1.0$ versus x_T at the parton level at 200 GeV. The square markers show the 2015 data from [16], whereas the triangle markers show the 2009 data from [6]. (b) A_{LL} for inclusive jets with $|\eta| < 0.9$ versus parton jet p_T based on 2012 data at 510 GeV [17]. The error bars show the size of the statistical uncertainties, whereas the boxes indicate the size of the systematic uncertainties. The yellow, pink and gray bands represent the common relative luminosity uncertainty. The curves show the expected A_{LL} values for the DSSV14 [2] and NNPDFpol1.1 [1] with the blue uncertainty band for the latter. The green curves in Fig. (b) show predictions from the 100 equally probable NNPDFpol1.1 replicas.

72 Figure 2 shows recent results on dijet A_{LL} for the same datasets. The asymmetry for di-
 73 jets versus M_{inv}/\sqrt{s} at the parton level at $\sqrt{s} = 200$ GeV and mid-pseudorapidity are pre-
 74 sented in Fig. 2a. It is shown for two different event topologies, $\text{sign}(\eta_1) = \text{sign}(\eta_2)$ and
 75 $\text{sign}(\eta_1) \neq \text{sign}(\eta_2)$, where 1 and 2 denote the two jets. The different topologies sample differ-
 76 ent regions of x . The same-sign events probe more asymmetric collisions with better-separated
 77 high- x and low- x distributions, while the opposite-sign events probe an intermediate- x range
 78 (see, e.g., Fig. 3 in Ref. [7]). For the 510 GeV results at mid-pseudorapidity, presented
 79 in 2b, individual jets in the dijet were sorted into the following three categories: forward
 80 ($0.3 < \eta < 0.9$), central ($|\eta| < 0.3$), and backward ($-0.9 < \eta < -0.3$). The final A_{LL} re-
 81 sults are presented for four dijet event topologies, namely, with forward-forward jets, forward-
 82 central jets, central-central jets, and forward-backward jets. The forward-forward and forward-
 83 central configurations probe the most asymmetric collisions down to $x \simeq 0.015$. The forward-
 84 forward and central-central events probe collisions with $|\cos \theta^*|$ near zero, whereas forward-
 85 central and forward-backward events are more sensitive to larger $|\cos \theta^*|$, where θ^* is the
 86 scattering angle in the center-of-mass frame of scattering partons. The preliminary results for
 87 the measurement at 510 GeV and intermediate pseudorapidity ($-0.8 < \eta < 1.8$) [19] are
 88 shown in Fig. 2c. The results are divided into three classes based on the pseudorapidities of
 89 the jets in the dijet pair: one jet in the east half of the BEMC ($-0.8 < \eta < 0$) or the west
 90 half of the BEMC ($0 < \eta < 0.8$) and the other jet in the EEMC ($0.8 < \eta < 1.8$), or both jets
 91 in the EEMC. The last category probes the most asymmetric collisions to x even below 0.015.
 92 In all the figures presented in this section, theoretical evaluations of A_{LL} for DSSV14 [2] and
 93 NNPDFpol1.1 [1] parton distribution functions are presented for comparison.

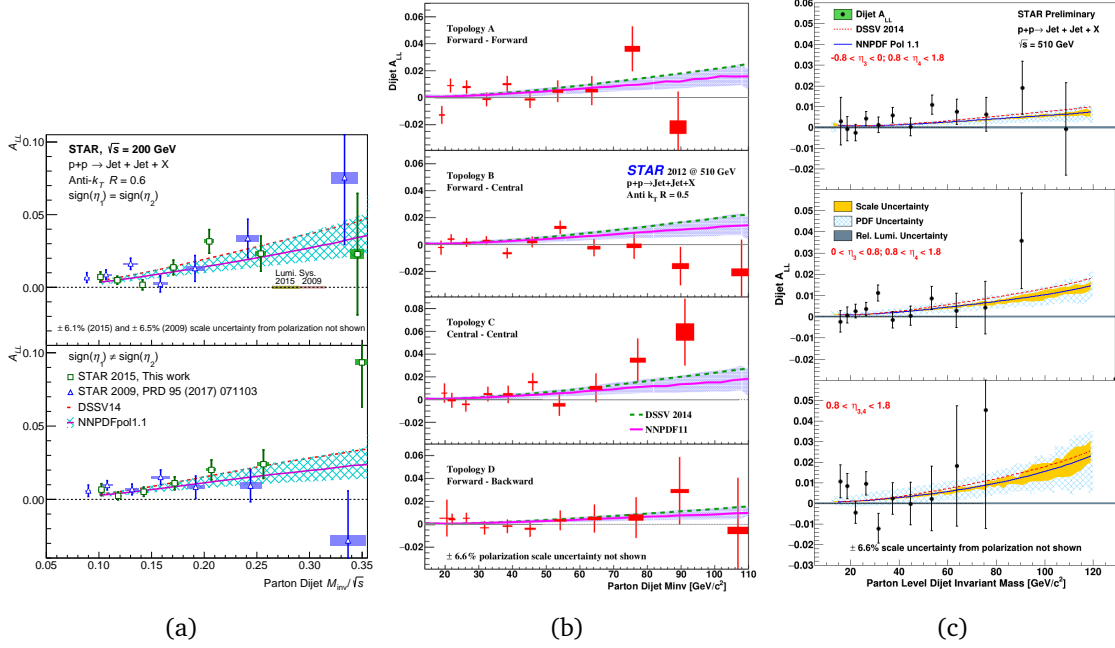


Figure 2: A_{LL} as a function of parton-level invariant mass for dijets from 2012 data at 510 GeV as well as 2009 and 2015 data at 200 GeV. Figure (a) presents A_{LL} versus M_{inv}/\sqrt{s} at 200 GeV for dijets with the $\text{sign}(\eta_1) = \text{sign}(\eta_2)$ (top) and $\text{sign}(\eta_1) \neq \text{sign}(\eta_2)$ (bottom) event topologies. The square markers show the 2015 data from [16], whereas the triangle markers show the 2009 data from [7]. Figure (b) presents results at 510 GeV from [17] for different event topologies in BEMC as described in the text. Figure (c) shows the preliminary results at 510 GeV obtained for the east BEMC-EEMC (top), west BEMC-EEMC (middle) and EEMC-EEMC (bottom) event topologies [19]. The error bars show the size of the statistical uncertainties, whereas the boxes indicate the size of the systematic uncertainties. In Fig. (c) only statistical uncertainties are presented. The curves represent theoretical evaluations of A_{LL} for DSSV14 [2] and NNPDFpol1.1 [1] parton distribution functions with the blue uncertainty band for the latter.

94 4 Summary

95 STAR has recently published results for inclusive jet and dijet longitudinal double-spin asym-
 96 metries at mid-pseudorapidity based on data collected in 2015 at 200 GeV [16] and 2012 at
 97 510 GeV [17]. These results build on the prior STAR measurements [6–8], with [6] providing
 98 the first evidence for positive polarization of the gluons in a polarized proton for $x > 0.05$
 99 upon inclusion in global analyses. The recent STAR results presented in these proceedings
 100 are in good agreement with the prior STAR measurements as well as the theoretical eval-
 101 uations from DSSV14 [2] and NNPDFpol1.1 [1]. The 2015 results with an approximately
 102 twice larger figure of merit and reduced systematic uncertainties compared to the prior data
 103 at $\sqrt{s} = 200$ GeV will provide one of the most stringent constraints on the magnitude and shape
 104 of the gluon helicity distribution for $x > 0.05$ when included in future global analyses of the
 105 polarized parton distribution functions. The first results at 510 GeV at mid-pseudorapidity
 106 and recent preliminary results at intermediate pseudorapidity based on 2012 data, as well as
 107 upcoming measurements based on 2013 data at 510 GeV with an integrated luminosity of
 108 $\mathcal{L} \simeq 250 \text{ pb}^{-1}$, will provide further constraints on $\Delta g(x, Q^2)$, especially in the region $x < 0.05$
 109 where $\Delta g(x, Q^2)$ is largely unconstrained in the prior global analyses. Since the Relativis-

110 tic Heavy Ion Collider has concluded the data taking with longitudinally polarized protons in
111 2015, the STAR data are anticipated to provide one of the most important insights to $\Delta g(x, Q^2)$
112 well into the future.

113 Acknowledgements

114 We thank the RHIC Operations Group and RCF at BNL. This work is supported by the U.S.
115 DOE Office of Science.

116 References

- 117 [1] E. R. Nocera, R. D. Ball, S. Forte, G. Ridolfi and J. Rojo, *A first unbiased global de-*
118 *termination of polarized PDFs and their uncertainties*, Nucl. Phys. B **887**, 276 (2014),
119 doi:[10.1016/j.nuclphysb.2014.08.008](https://doi.org/10.1016/j.nuclphysb.2014.08.008).
- 120 [2] D. de Florian, R. Sassot, M. Stratmann and W. Vogelsang, *Evidence for po-*
121 *larization of gluons in the proton*, Phys. Rev. Lett. **113**(1), 012001 (2014),
122 doi:[10.1103/PhysRevLett.113.012001](https://doi.org/10.1103/PhysRevLett.113.012001).
- 123 [3] D. de Florian, G. A. Lucero, R. Sassot, M. Stratmann and W. Vogelsang, *Monte Carlo*
124 *sampling variant of the DSSV14 set of helicity parton densities*, Phys. Rev. D **100**(11),
125 114027 (2019), doi:[10.1103/PhysRevD.100.114027](https://doi.org/10.1103/PhysRevD.100.114027).
- 126 [4] M. Salimi-Amiri, A. Khorramian, H. Abdolmaleki and F. I. Olness, *Impact of recent COM-*
127 *PASS data on polarized parton distributions and structure functions*, Phys. Rev. D **98**(5),
128 056020 (2018), doi:[10.1103/PhysRevD.98.056020](https://doi.org/10.1103/PhysRevD.98.056020).
- 129 [5] N. Sato, W. Melnitchouk, S. E. Kuhn, J. J. Ethier and A. Accardi, *Iterative Monte Carlo*
130 *analysis of spin-dependent parton distributions*, Phys. Rev. D **93**(7), 074005 (2016),
131 doi:[10.1103/PhysRevD.93.074005](https://doi.org/10.1103/PhysRevD.93.074005).
- 132 [6] L. Adamczyk *et al.*, *Precision Measurement of the Longitudinal Double-spin Asymmetry for*
133 *Inclusive Jet Production in Polarized Proton Collisions at $\sqrt{s} = 200$ GeV*, Phys. Rev. Lett.
134 **115**(9), 092002 (2015), doi:[10.1103/PhysRevLett.115.092002](https://doi.org/10.1103/PhysRevLett.115.092002).
- 135 [7] L. Adamczyk *et al.*, *Measurement of the cross section and longitudinal double-spin asym-*
136 *metry for di-jet production in polarized pp collisions at $\sqrt{s} = 200$ GeV*, Phys. Rev. D **95**(7),
137 071103 (2017), doi:[10.1103/PhysRevD.95.071103](https://doi.org/10.1103/PhysRevD.95.071103).
- 138 [8] J. Adam *et al.*, *Longitudinal double-spin asymmetries for dijet production at intermediate*
139 *pseudorapidity in polarized pp collisions at $\sqrt{s} = 200$ GeV*, Phys. Rev. D **98**(3), 032011
140 (2018), doi:[10.1103/PhysRevD.98.032011](https://doi.org/10.1103/PhysRevD.98.032011).
- 141 [9] D. Kalinkin, *Measurement of Mid-rapidity Inclusive Jet Cross Section in pp Collisions at*
142 *$\sqrt{s} = 200$ GeV*, In *APS Division of Nuclear Physics Meeting* (2020).
- 143 [10] D. Kalinkin, *Measurement of Mid-rapidity Inclusive Jet Cross Section in pp Collisions at*
144 *$\sqrt{s} = 200$ GeV*, In *XXVIII International Workshop on Deep-Inelastic Scattering and Related*
145 *Subjects* (2021).
- 146 [11] M. Anderson *et al.*, *The Star time projection chamber: A Unique tool for studying high*
147 *multiplicity events at RHIC*, Nucl. Instrum. Meth. A **499**, 659 (2003), doi:[10.1016/S0168-](https://doi.org/10.1016/S0168-9002(02)01964-2)
148 [9002\(02\)01964-2](https://doi.org/10.1016/S0168-9002(02)01964-2).

- 149 [12] M. Beddo *et al.*, *The STAR barrel electromagnetic calorimeter*, Nucl. Instrum. Meth. A
150 **499**, 725 (2003), doi:[10.1016/S0168-9002\(02\)01970-8](https://doi.org/10.1016/S0168-9002(02)01970-8).
- 151 [13] C. Allgower *et al.*, *The STAR endcap electromagnetic calorimeter*, Nucl. Instrum. Meth. A
152 **499**, 740 (2003), doi:[10.1016/S0168-9002\(02\)01971-X](https://doi.org/10.1016/S0168-9002(02)01971-X).
- 153 [14] W. Llope *et al.*, *The STAR Vertex Position Detector*, Nucl. Instrum. Meth. A **759**, 23 (2014),
154 doi:[10.1016/j.nima.2014.04.080](https://doi.org/10.1016/j.nima.2014.04.080).
- 155 [15] C. Adler, A. Denisov, E. Garcia, M. J. Murray, H. Strobele and S. N. White, *The RHIC*
156 *zero degree calorimeter*, Nucl. Instrum. Meth. A **470**, 488 (2001), doi:[10.1016/S0168-](https://doi.org/10.1016/S0168-9002(01)00627-1)
157 [9002\(01\)00627-1](https://doi.org/10.1016/S0168-9002(01)00627-1).
- 158 [16] M. Abdallah *et al.*, *Longitudinal double-spin asymmetry for inclusive jet and dijet production*
159 *in polarized proton collisions at $\sqrt{s} = 200$ GeV*, Phys. Rev. D **103**(9), L091103 (2021),
160 doi:[10.1103/PhysRevD.103.L091103](https://doi.org/10.1103/PhysRevD.103.L091103), [2103.05571](https://arxiv.org/abs/2103.05571).
- 161 [17] J. Adam *et al.*, *Longitudinal double-spin asymmetry for inclusive jet and dijet pro-*
162 *duction in pp collisions at $\sqrt{s} = 510$ GeV*, Phys. Rev. D **100**(5), 052005 (2019),
163 doi:[10.1103/PhysRevD.100.052005](https://doi.org/10.1103/PhysRevD.100.052005).
- 164 [18] B. B. Abelev *et al.*, *Charged jet cross sections and properties in proton-proton collisions at*
165 *$\sqrt{s} = 7$ TeV*, Phys. Rev. D **91**(11), 112012 (2015), doi:[10.1103/PhysRevD.91.112012](https://doi.org/10.1103/PhysRevD.91.112012).
- 166 [19] J. Kwasizur, *Longitudinal Double-Spin Asymmetries for Dijet Production at Intermediate*
167 *Pseudorapidity in Polarized Proton-Proton Collisions at $\sqrt{s} = 510$ GeV*, In *APS Division of*
168 *Nuclear Physics Meeting* (2020).